APEM journal
Advances in Production Engineering & Management
Volume 20 | Number 4 | December 2025 | pp 423–433
https://doi.org/10.14743/apem2025.4.549
ISSN 1854-6250
Journal home: apem-journal.org
Original scientific paper

Influence of cutting-edge tip geometry on the tool–workpiece electrical contact resistance

Murata, M.[a,*], **Cao, W.**[b]

[a]Department of Mechanical Engineering, Kyushu Sangyo University, Fukuoka, Japan
[b]The Graduate School of Engineering, Kyushu Sangyo University, Fukuoka, Japan

ABSTRACT

It is well established that the electrical resistance generated at the contact interface between dissimilar metals is strongly correlated with the actual contact area. By leveraging this phenomenon in cutting operations, we have successfully achieved in-process identification of flank wear width during machining. The method has shown particularly favourable performance under finishing conditions involving interrupted cutting, where tool monitoring is generally considered challenging. However, cutting operations employ a wide range of tool geometries, cutting parameters, and machining configurations, and it remains unclear whether the proposed approach is universally applicable across these variations. To address this issue, the present study focuses on turning, a process in which the tool–workpiece contact time is relatively long, and investigates the applicability of the method to diverse cutting geometries. Specifically, we examine how differences in tool geometry and the chip–rake-face contact area influence the electrical contact resistance between the tool and the workpiece. The results indicate that, for unused tools, variations in nose radius do not affect the electrical contact resistance measured at the tool–workpiece interface. In contrast, the contact between the flowing chip and the rake face is strongly dependent on rake angle. Consequently, for tools with negative rake angles, chip–rake-face interaction was found to have a pronounced influence on the electrical contact resistance at the tool–workpiece interface.

ARTICLE INFO

Keywords:
Tool wear detection;
Contact resistance;
In-process monitoring;
Real time evaluation;
Rake angle;
Nose radius

**Corresponding author:*
murata@ip.kyusan-u.ac.jp
(Murata, M.)

Article history:
Received 1 December 2025
Revised 6 December 2025
Accepted 13 December 2025

1. Introduction

Employment in Japan's manufacturing sector has shown a declining trend in recent years. According statistical data from 2002 onward, the number of people employed in the manufacturing industry has decreased from 12.02 million in 2002 to 10.55 million in 2023, a decline of approximately 1.5 million. In particular, the number of young workers aged 34 and under has shown a significant decline. Since 2002, the number of young employees has decreased by 1.25 million. In contrast, the number of elderly workers aged 65 and over has been increasing. While there were 580,000 elderly workers in 2002, this number rose to 880,000 by 2023 [1-3].

Statistical data published by the Small and Medium Enterprise Agency of Japan indicate that the labour shortages in small and medium-sized manufacturing enterprises have become increasingly severe since 2013. As a result, elderly workers, who are supposed to serve as mentors for younger employees by transferring their technical skills, are unable to step away from front-line operations. This situation has led to significant difficulties in fostering the next generation of skilled workers. Evidence from a survey by the Ministry of Health, Labour and Welfare of Japan

[4] further substantiates this issue, with 61.8 % of responding companies indicating a lack of personnel capable of instructing young-er workers. These findings statistically validate the previously anecdotal sense of a growing shortage of skilled labour in Japan. This challenge is equally evident in the field of machining, particularly in cutting processes [5-9].

In contrast, many contemporary consumer products rely on molds for mass production. Mold fabrication is generally carried out using machining centres, with machining times ranging from several hours to several days, depending on the intricacy of the design. At present, monitoring of cutting conditions during machining is predominantly conducted through human judgment. Nevertheless, continuous human supervision throughout prolonged machining processes is impossible due to labour hour constraints and the ongoing shortage of human resources. In particular, during the finishing cutting process, due to cutting conditions such as high spindle speeds, extremely small feed rates, and minimal depths of cut, it is almost impossible for operators to detect abnormal sounds or vibrations emanating from the machine during cutting. Therefore, the implementation of automatic condition monitoring technology during cutting operations is essential.

To date, we have conducted studies on the identification of optimal cutting tool change timing during intermittent cutting processes. We have achieved in-process tool wear detection during the cutting process by measuring the changes in tool–workpiece contact electrical resistance as an indicator of tool wear [10-12]. This detection signal is in excellent agreement with Holm's con-tact theory, which addresses the contact electrical resistance between dissimilar metals [13, 14]. By applying Holm's contact theory, we derived an identification formula for the flank wear width of the tool, enabling its estimation from the tool–workpiece contact electrical resistance with a certain degree of accuracy [15]. Furthermore, by revising the measurement sequence of the tool–workpiece contact electrical resistance, we were able to detect tools with a minimum diameter of 6.0 mm at a cutting speed of 100 m/min [16].

Various experimental techniques have been proposed for detecting tool wear, including conventional monitoring approaches such as cutting-force measurement, machine-vibration monitoring, monitoring of AC spindle-motor slip, and motor-current monitoring, among others. These methods generally exhibit higher sensitivity under heavy cutting conditions. In contrast, the present method becomes more sensitive in regions where the tool–workpiece contact area is small. Accordingly, it is particularly well suited for determining the tool-replacement timing under finishing conditions with small depths of cut, where the flank-wear width remains relatively small [10]. These experiments were conducted using uncoated carbide cutting edges under dry cutting conditions, with results based on a single tool geometry. In practical cutting processes, a wide range of conditions are applied, including various tool types, coating types, and the use of cutting fluids (such as water-soluble or oil-based fluids).

As the next step in our investigation, we need to examine whether the tool–workpiece contact electrical resistance measurement can be accurately performed under these various machining conditions, whether the measurement accuracy is affected, and whether it maintains a consistent relationship with the flank wear width of the tool, as observed in previous studies. In the previous experiments, as mentioned earlier, testing was conducted under intermittent cutting conditions using a milling machine. In intermittent cutting, the contact time between the cutting edge and the workpiece is shortened. As a result, we have been struggling with the reduction in measurement time due to the slow response speed of the detection waveform.

Therefore, in this experiment, to focus solely on the effects of tool geometry, a lathe, which operates under continuous cutting conditions, was used. This eliminates the need to consider the short measurement time. For the reasons mentioned above, an investigation was conducted to examine how the difference in tool nose radius affects the tool–workpiece contact electrical resistance during outer diameter turning. Additionally, an investigation was also conducted to examine how the presence or absence of a chip breaker, i.e., the difference in tool-chip contact length, affects the tool–workpiece contact electrical resistance, and the results are presented here.

2. Measurement principle and experimental setup

The measurement of tool–workpiece contact electrical resistance is performed using the DC two-terminal method. Fig. 1 shows the measurement principle. R_k is the tool–workpiece electrical contact resistance, while R_1 is the specific resistance of the measurement circuit. $E_1$is the tool–workpiece thermoelectromotive force (E.M.F.) caused by the contact between the tool and the workpiece.

The current generator produces a constant current of 4 A using a 12 V DC switching power supply and a resistance of 3 Ω. The electrical resistance values of R_k and R_1 are on the order of several milliohms; therefore, they have no effect on the variation in the constant-current value. A current of 4 A can be turned ON and OFF using the analogue switch SW1, which is composed of three power MOSFETs and has arbitrary timing. During cutting, that is, when the tool and workpiece are in contact, a closed-loop circuit is formed and a constant current I of 4 A is applied. The voltage drop is measured at this time, and by applying Ohm's law, the contact electrical resistance between the tool and the workpiece is obtained.

The voltage drop value varies depending on the contact area between the tool and the workpiece. Specifically, as the flank wear width increases, the contact area between the tool and the workpiece also expands, resulting in a decrease in the contact electrical resistance in accordance with Holm's contact theory. On the other hand, since the tool and the workpiece are typically made of different metals, a thermoelectromotive force E_1(E.M.F.) is generated due to the cutting heat. The voltage drop waveform measured at this time includes the tool–workpiece E.M.F. From the voltage drop waveform obtained during the tool–workpiece contact electrical resistance measurement, the steady-state value of the tool–workpiece E.M.F. is subtracted in order to obtain the true tool–workpiece contact electrical resistance value R_k. However, since the measurement principle is based on the DC two-terminal method, the measured electrical resistance value includes the resistance of the wiring R_1.

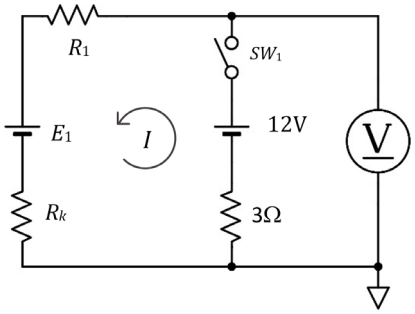

Fig. 1 Equivalent circuit of measurement system

Fig. 2 shows an example of the waveform obtained during previous intermittent cutting experiments and the corresponding signal-processing sequence. When the tool and the workpiece come into contact, the tool–workpiece E.M.F. waveform first rises. Based on previous experiments, the tool–workpiece E.M.F. reaches a steady state within approximately 1.5 to 2.0 ms. Thus, the waveform is sampled for 1 ms, beginning 3 ms after the onset of the E.M.F., and the average voltage is stored as the steady E.M.F. After that, a constant current of 4 A is applied to the closed-loop circuit. Although the waveform initially exhibits a large overshoot, it reaches a steady value after approximately 2.0 ms. The steady-state voltage drop is then subtracted in real time by the previously stored steady-state E.M.F., allowing for the in-process measurement of the tool–workpiece contact electrical resistance.

In this experiment, to investigate how the cutting edge geometry affects the tool–workpiece contact electrical resistance, an experimental setup based on this principle was incorporated into a lathe for continuous cutting, where the contact time between the tool and the workpiece is longer. Fig. 3 shows the block diagram of this setup. By grounding the lathe body, the system is connected in such a way that the influence of external noise is minimized. When the spindle stops, all metal components, including the tool and the workpiece, are in contact, and therefore the tool and the workpiece are at the same potential.

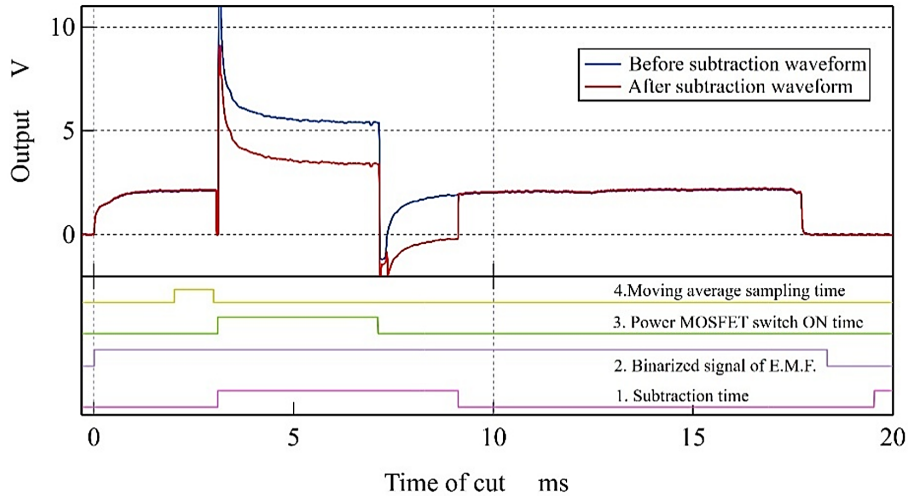

Fig. 2 Measured waveforms and timing of signal process in intermittent cutting

It has been reported that, during rotation, a lubricant film is formed at the contact points between the inner race, rolling elements, cage, and outer race of the bearing. As a result, an electrical resistance exists between the inner and outer races [17]. This electrical resistance has a value significantly larger than the tool–workpiece contact electrical resistance. Therefore, during spindle rotation, the workpiece can be considered almost isolated from the ground potential. This is also evident from the waveforms obtained later, where the tool–workpiece E.M.F. is generated during cutting.

The electrical connection to the rotating workpiece is made through the chuck and the spindle sleeve and is connected to a rotary contact mounted at the end of the spindle sleeve. In past experiments, we examined the differences in output waveforms obtained using three types of rotating contacts: a commercially available liquid-metal contact that uses mercury, a custom-built liquid-metal contact employing a gallium alloy, and a commercially available slip ring that uses solid metals as the contact material. The results showed that when a commercial slip ring is used, a thermoelectric E.M.F. is generated due to the frictional heat produced during rotation, because the metals used for the contacts are dissimilar. In addition, a typical slip ring presses a brush against the rotor using spring force; however, this mechanism cannot completely eliminate variations in contact force caused by eccentricity of the rotating shaft. Consequently, the E.M.F. output from the slip ring appears as a wavy waveform synchronized with the rotational speed.

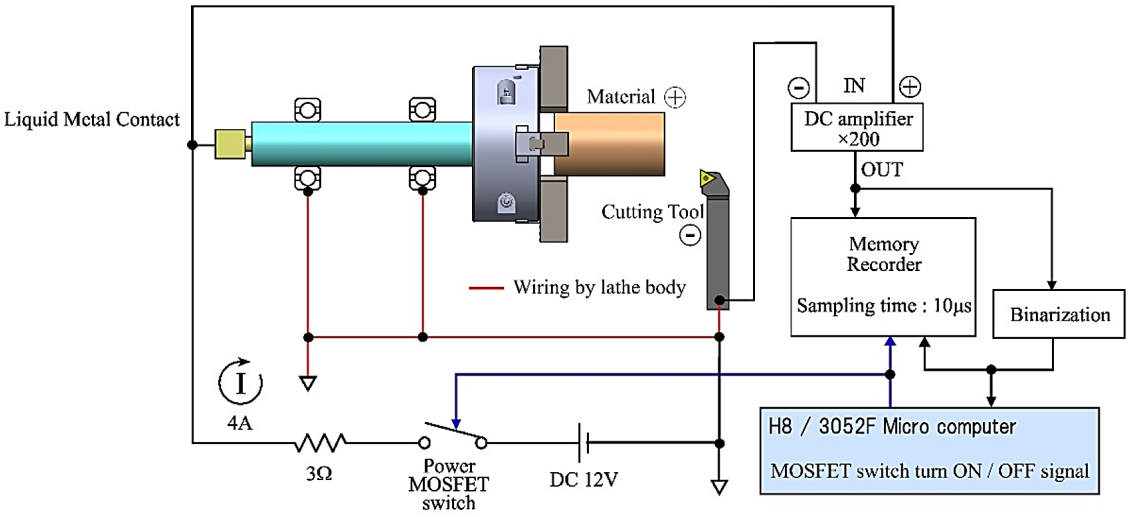

Fig. 3 Block diagram of experimental setup

On the other hand, it was found that the output waveforms obtained using the commercial mercury-based liquid rotary contact and the custom-built gallium-alloy liquid-metal contact exhibited no significant differences [16]. However, because mercury is a metal that can pose risks to human health, its use requires sufficient caution. Therefore, in the present study, a liquid-metal rotary contact utilizing a gallium alloy (Gallium 68.5 %, Indium 21.5 %, Tin 10.0 %) was selected. As a result, it can be used without issue up to the maximum spindle speed of 2000 min^{-1} in the lathe used for the experiment.

A constant current of 4 A is applied to the closed loop by turning on a switch made of a MOSFET after sufficient time has passed following the contact between the tool and the workpiece and the generation of the E.M.F. The voltage drop waveform observed after turning on both the E.M.F. and the constant current is amplified 200 times by a DC amplifier and then recorded in the data recorder along with the control signals.

3. Experiment method and experimental conditions

A total of five cutting tools with distinct cutting-edge geometries were prepared for the experiments. Four of these tools featured negative rake angles and consisted of uncoated carbide throw-away inserts without chip breakers but with different nose radii (0.4, 0.8, and 1.2 mm), as well as a 0.4-mm-nose-radius insert equipped with a chip breaker.

Many of the cutting tools used in actual machining environments are coated with various materials on their cutting edges to extend tool life. The authors have previously conducted tool-wear experiments using coated end mills to examine how different coating materials influence the tool–workpiece electrical contact resistance [18]. The results showed that the type of coating material has a substantial effect on the E.M.F. generated at the tool–workpiece interface. Depending on the combination of coating material and workpiece material, both the magnitude and the polarity of the generated voltage vary. In contrast, it was also confirmed that the influence of tool coatings on the tool–workpiece electrical contact resistance is very small. This result is consistent with reports in the literature indicating that, when the applied normal load exceeds 10 N and the thickness of the thin film deposited on the substrate is less than 10 μm, the electrical resistivity of the film does not affect the electrical contact resistance [19]. In the present study, in order to investigate the effect of tool geometry on the electrical contact resistance between the tool and the workpiece, uncoated inserts were selected for all cutting edges used in the experiments.

The fifth tool employed a positive rake angle and a 0.4-mm-nose-radius insert without a chip breaker. Cutting experiments were conducted using all of these tools. All inserts were equilateral triangular types with a corner angle of 60 °, manufactured by Tungaloy. The carbide grade was TH10 (Tungaloy designation), and none of the inserts had surface coatings.

The tool holders used in all experiments had an approach angle of 91 °, with rake angles of −5 ° for the negative-rake configurations and +5 ° for the positive-rake configuration. It is standard practice to mount inserts with a breaker piece placed on the cutting edge when using a tool holder with a positive rake angle. However, in the present experiments, it was necessary to eliminate the influence of measurement variations caused by contact between the insert and the breaker piece. Therefore, the insert was fixed to the holder without using a breaker piece.

The cutting speed V was set to 80, 100, and 150 m/min for each cutting edge. For each cutting speed, the depth of cut t was varied from 0.1 mm to 1.2 mm, and cutting experiments were conducted. The workpiece used was chromium-molybdenum steel with a diameter of 50 mm (JIS: SCM420, ASTM: AISI 4130, ISO: 25CrMo4). Before each cutting operation, the outer diameter of the workpiece was measured, and the spindle speed was set to ensure that the outer diameter of the workpiece achieved the cutting speed corresponding to each setting.

The feed rate per spindle revolution f was kept constant at 0.1 mm/rev for all conditions, and the cutting was performed under dry cutting conditions without the use of cutting fluids. The experimental conditions used in this experiment are summarized in Table 1.

Table 1 Experimental setup

	Insert #1	Insert #2	Insert #3	Insert #4	Insert #5
Nose radius	0.4 mm	0.8 mm	1.2 mm	0.4 mm	0.4 mm
Chip breaker shape	-			P  [20]	-
Insert dimension	60 ° equilateral triangle				
Insert photos	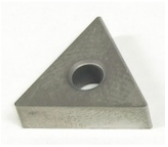		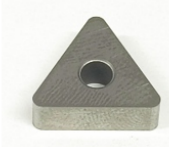		
Insert manufacture	Tungaloy				
Insert material	Cemented carbide (Tungaloy model number TH10)				
Insert coating	-				
Tool holder shape	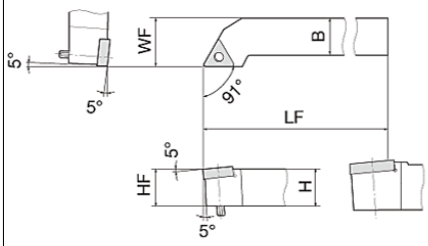 For Insert #1 to #4 [20]			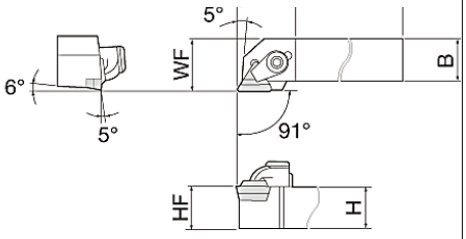 For Insert #5 only [20]	
Rake angle	−5 °			+5 °	
Cutting edge angle	91 °			91 °	
Cutting speed V	80 m/min, 100 m/min, 150 m/min				
Work material	50 mm in diameter Chrome-molybdenum steel (JIS: SCM420, ASTM: AISI 4130, ISO: 25CrMo4)				
Depth of cut t	0.1, 0.2, 0.3, 0.4, 0.5, 0.6, 0.7, 0.8, 1.0, 1.2 mm				
Feed rate f	0.1 mm/rev				
Cutting lubricant	(Dry cutting)				

4. Experimental results

Fig. 4 shows an example of the output waveform obtained in this experiment. This waveform was obtained with a cutting speed $V = 100$m/min, a depth of cut $t = 0.5$mm, and Tool insert #1. The memory recorder used in this experiment was set to a sampling interval of 10 μs, allowing it to record waveforms for 20 seconds.

Fig. 4 first shows the waveform recorded during the idle rotation of the spindle. The spiky noise observed at this time is considered to be caused by the E.M.F. generated by instantaneous metal contact, such as that occurring in the spindle bearing. However, it is clear from both the subsequent E.M.F. waveform and the voltage drop waveform that this spiky noise does not affect the measured waveforms.

Subsequently, when the tool and the workpiece make contact, the tool–workpiece E.M.F. rises (the enlarged section: Fig. 4a). The workpiece used in this experiment was directly cut from a long bar of material using a saw, and thus the material's end face is not perpendicular to the spindle rotation axis. As a result, the waveform at the beginning of cutting resembles that of intermittent cutting.

Subsequently, at arbitrary timing, a constant current of 4 A is passed through the closed-loop circuit formed by the contact between the tool and the workpiece. At this point, the waveform

initially experiences a large overshoot but quickly reaches a steady-state value (the enlarged section: Fig. 4b). The steady-state value at this point corresponds to the voltage drop waveform due to the tool–workpiece contact electrical resistance. However, as mentioned earlier, this waveform also includes the tool–workpiece E.M.F. Thus, by subtracting the average value of the tool–workpiece E.M.F. from this waveform, the true voltage drop waveform can be obtained.

In this experiment, the average E.M.F. is taken as the arithmetic mean of the E.M.F. during the one second before applying the constant current. After that, the value of the voltage drop caused by the contact electrical resistance was determined by subtracting the average value of the E.M.F. waveform from the arithmetic mean of the voltage drop waveform measured during one second after applying the constant current. After dividing this value by 200, the true tool–workpiece contact electrical resistance was calculated using Ohm's law.

Since the measurement uses the DC two-terminal method, the wiring resistance is included in the measured value. However, as long as the same machine is used, this wiring resistance remains constant and does not need to be considered when measuring changes in contact electrical resistance. When the constant current is turned off after a certain period, the waveform first undershoots and then returns to the steady-state value of the tool–workpiece E.M.F. (the enlarged section: Fig. 4c).

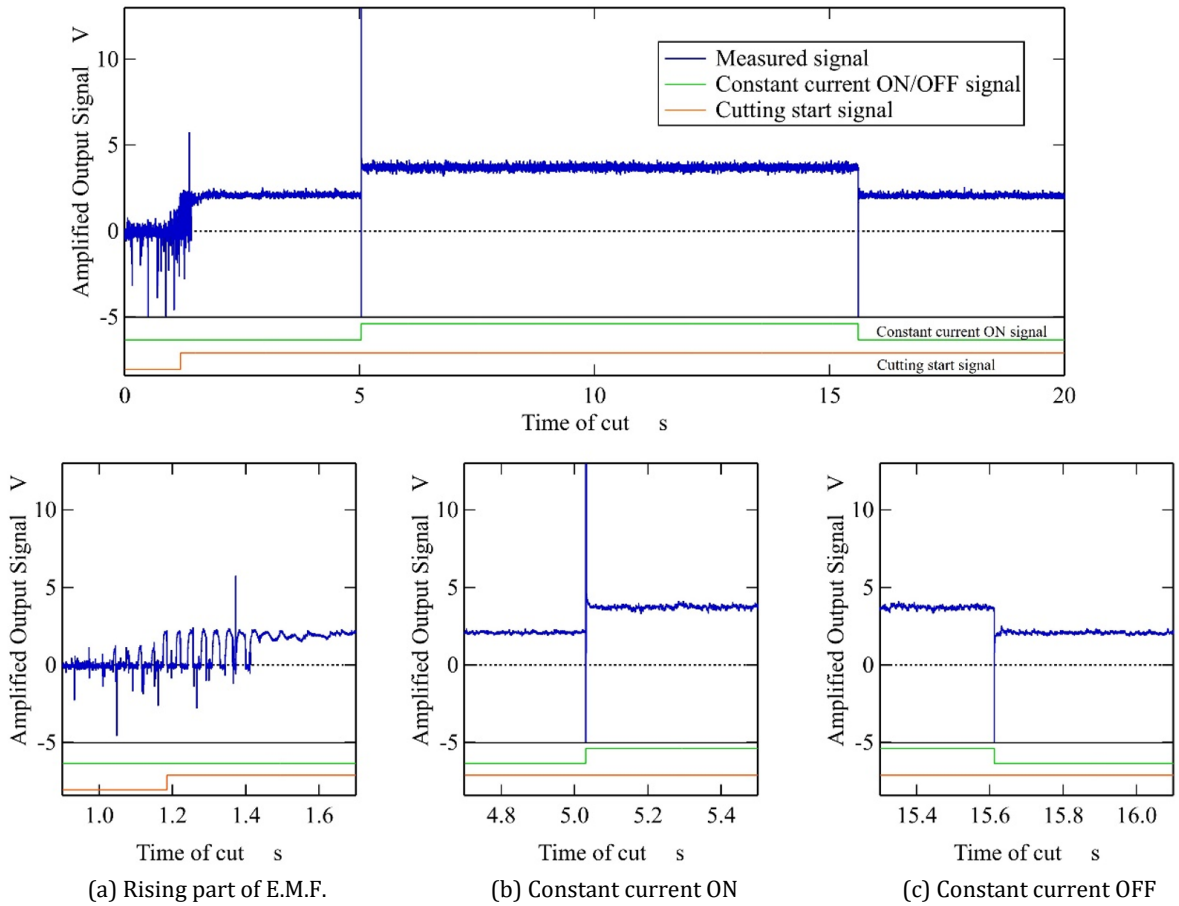

Fig. 4 Measurement waveform and enlarged view of each timing

5. Discussion

5.1 Effect of cutting speed

Fig. 5 shows the relationship between the depth of cut and the variation in tool–workpiece electrical contact resistance for each cutting edge. Each graph overlays the measurement results obtained at three different cutting speeds for the corresponding cutting edge. Among these graphs, for the negative-rake-angle inserts without a chip breaker (Insert #1, #2, and #3), it can be observed that the measured values at a cutting speed of V = 150 m/min tend to be slightly

lower. Electrical resistivity varies with temperature and generally increases as temperature rises. Since cutting temperature typically increases with cutting speed, a higher cutting speed would normally be expected to result in higher electrical resistivity. Focusing on the results at cutting speeds of V = 80 m/min and 100 m/min, Insert #1 and #2 exhibit larger resistance values at V = 80 m/min than at V = 100 m/min, whereas Insert #3 shows the opposite trend. Furthermore, for Insert #4 and #5, no clear differences in electrical contact resistance due to cutting speed are observed. From these observations, it can be concluded that the cutting speed does not significantly influence the electrical contact resistance between the tool and the workpiece.

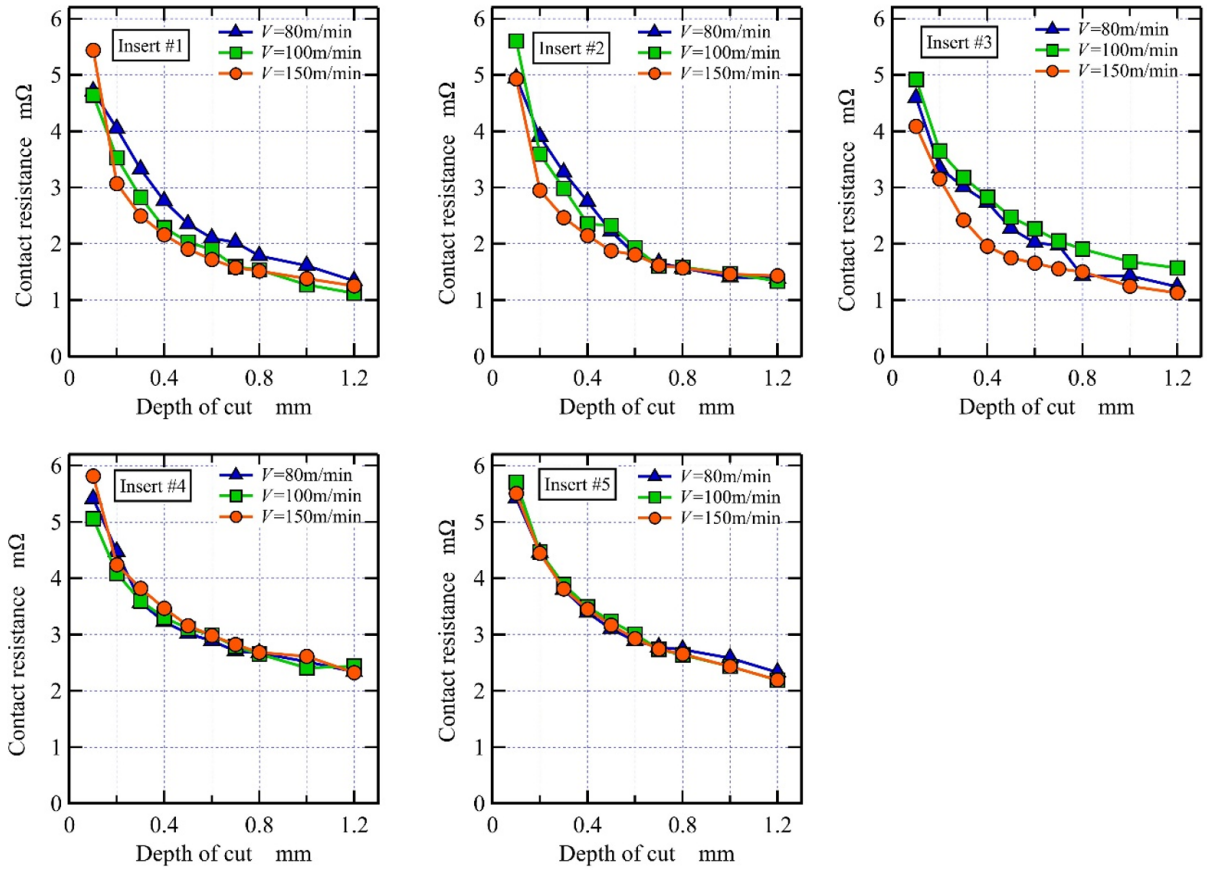

Fig. 5 Relationship between depth of cut and tool–workpiece contact resistance for each cutting edge geometry

5.2 Effect of nose radius

Next, the tool–workpiece electrical contact resistance obtained at each cutting speed was compared with respect to differences in nose radius. Fig. 6 shows the variation in electrical contact resistance for Insert #1, #2, and #3 at each cutting speed.

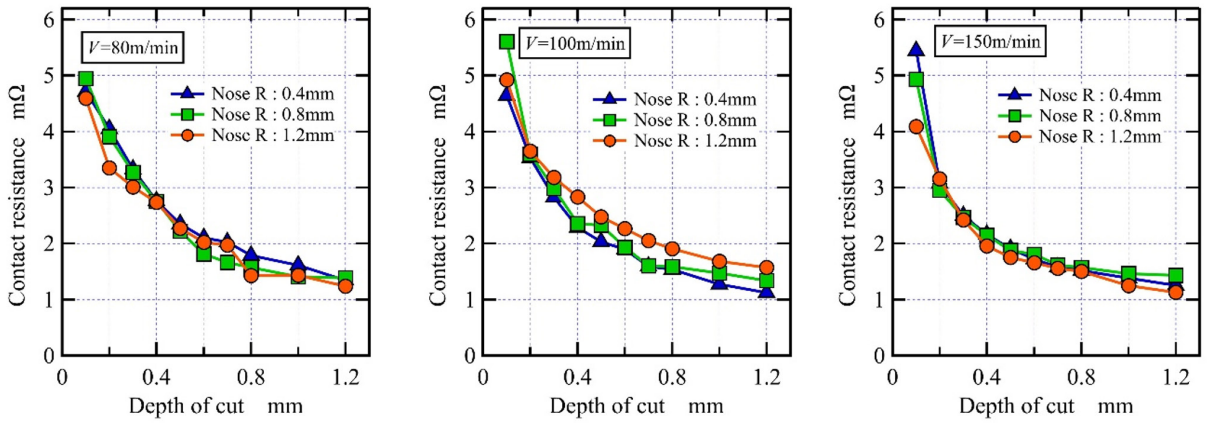

Fig. 6 Relationship between depth of cut and tool–workpiece contact resistance for each nose radius

From this figure, it can be seen that the difference in nose radius at the cutting edge does not affect the tool tool–workpiece workpiece electrical contact resistance. Geometrically, the size of the nose radius influences the contact area between the tool rake face and the workpiece only during the very first revolution, when the cutting edge initially engages with the material. Thereafter, the tool–workpiece contact area S becomes $f \times t$ deter-mined solely by the feed rate f and the depth of cut t, regardless of the nose radius. The present experimental results are considered to clearly reflect this behaviour.

5.3 Effect of chip–tool contact due to differences in rake angle

Finally, the influence of the tool rake angle on the tool–workpiece electrical contact resistance is examined. As shown in Table 1, Insert #1, #2, and #3 have a negative rake angle of −5 °. Although Insert #4 uses the same tool holder as Insert #1 to #3 and therefore has an overall negative rake angle, the cutting edge is equipped with a chip breaker with a 30 ° slope. Consequently, as long as the feed per revolution f (mm/rev) does not exceed the width of this chip breaker, the effective rake angle becomes +25 °. Insert #5 does not have a chip breaker, but the tool holder provides a positive rake angle of +5 °.

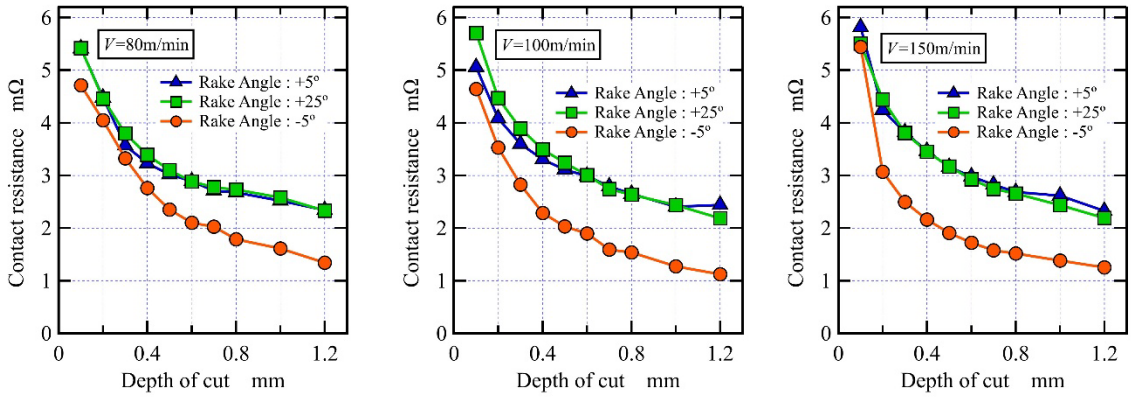

Fig. 7 Relationship between depth of cut and tool–workpiece contact resistance for each rake angle

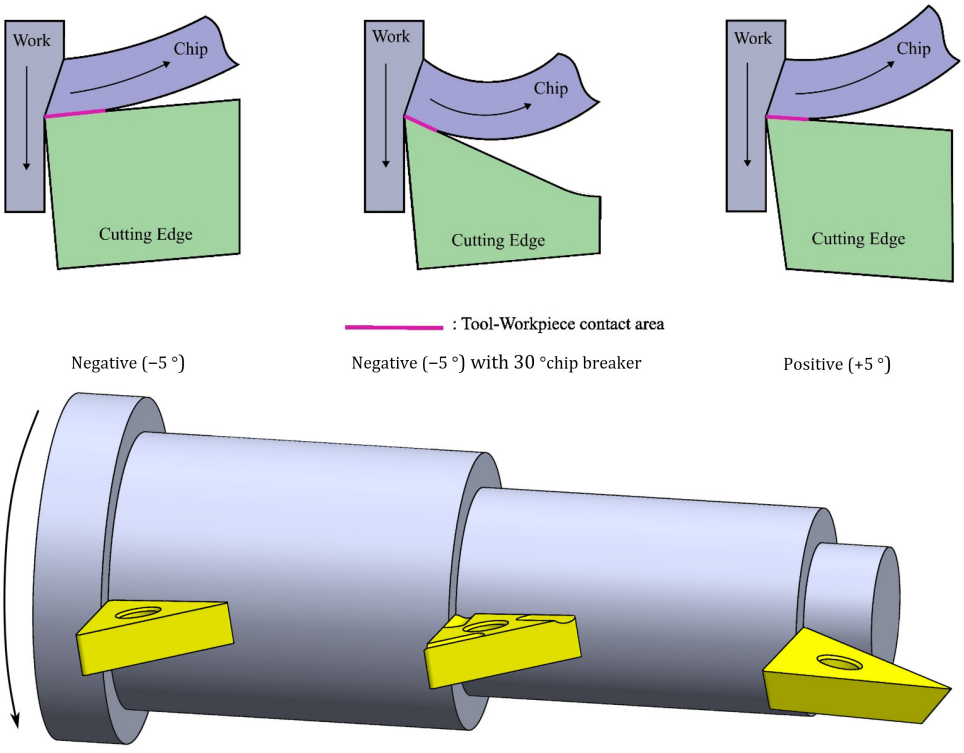

Fig. 8 Conceptual diagram of the contact area between the tool and the chip depending on the rake angle

Fig. 7 shows the relationship between the depth of cut and electrical contact resistance at each cutting speed for Insert #1, #4, and #5, all of which have the same nose radius. At all cutting speeds, a clear difference between positive and negative rake angles is observed. As illustrated conceptually in Fig. 8, when the rake angle is positive, the generated chip curls and is discharged with minimal contact with the rake face. In contrast, when the rake angle is negative, the chip is forced to remain in contact with the rake face over a certain distance, even while curling. This behaviour is also supported by FEM analyses reported in the literature [21, 22], which demonstrate the differences in chip flow associated with variations in rake angle.

6. Conclusion

In order to achieve in-process identification of cutting tool life, the variation in tool–workpiece electrical contact resistance, which serves as a highly effective detection signal, was investigated with respect to differences in cutting-edge geometry. The results revealed that neither cutting speed nor nose radius has a significant effect on the electrical contact resistance between the tool and the workpiece. On the other hand, a substantial difference in measured electrical contact resistance was observed between positive and negative rake angles.

In turning operations, most commercially available throw-away holders for external machining are designed with negative rake angles. However, the use of inserts without chip breakers, as employed in this experiment, is rarely applied in general machining due to considerations of chip evacuation. Therefore, when using inserts with chip breakers, it is not necessary to account for a reduction in electrical contact resistance caused by chip contact with the rake face.

The machining scenario targeted in this study is the determination of the appropriate tool replacement timing during long-duration machining of molds, performed on machining centres. In intermittent machining, particularly in end-mill operations, the rake angle is always positive; therefore, the influence of chip contact on the rake face in this method does not need to be considered.

On the other hand, as mentioned earlier, cutting conditions in cutting processes are highly diverse. Therefore, it will be necessary to continue examining whether the proposed method can accommodate a wider range of conditions, such as the presence or absence of cutting fluids, the influence of different tool-coating materials on the tool–workpiece electrical contact resistance, and variations in workpiece material.

References

[1] Statistics Bureau of Japan, Ministry of Internal Affairs and Communications, Japan. The survey results of the labour force, from *https://www.stat.go.jp/english/data/roudou/result.html*, accessed November 29, 2025.

[2] Ministry of Economy, Trade and Industry, Japan (2025). 2025 Manufacturing white paper, (in Japanese), from *https://www.meti.go.jp/report/whitepaper/mono/2025/pdf/all.pdf*, accessed November 29, 2025.

[3] The Small and Medium Enterprise Agency (2025). 181st small and medium enterprise business survey, (in Japanese), from *https://www.chusho.meti.go.jp/koukai/chousa/keikyo/keikyo/181sokuhou.pdf*, accessed November 29, 2025.

[4] Ministry of Health, Labour and Welfare, Japan (2023). Human resources development basic survey: summary of results 2023, (in Japanese), from *https://www.mhlw.go.jp/content/11801500/001283508.pdf*, accessed November 29, 2025.

[5] Human Resources Development Research Center at Polytechnic University (2002). Supporting off-JT for highly skilled expertise and OJT: A research report on skill development through OJT, (in Japanese), *Polytechnic University Human Resources Development Research Center Research Report*, No. 110, 1-220, from *https://www.tetras.uitec.jeed.go.jp/research/detail?id=422*, accessed November 29, 2025.

[6] Hirayama, T. (2025). The significance and technology of manufacturing AI and full automation in metal parts manufacturing, (in Japanese), *Die and Mold Technology,* Vol. 40, No. 4, 28-31.

[7] Yukawa, K., Warisawa, S. (2013). An application to personnel training by the visualization of the expert skills in machine tool industries, (in Japanese), *International Business and Management Forum,* Vol. 24, 135-148, doi: 10.1299/jsmemsd.2011.67.

[8] Unno, K. (2015). Support and promotion of the skill succession by utilizing expert skilled workers, (in Japanese), *Journal of the Japan Society for Precision Engineering,* Vol. 81, No. 1, 30-33, doi: 10.2493/jjspe.81.30.

[9] Fujimoto, M. (2008). Fostering technicians and engineers in the manufacturing industry, (in Japanese), *Business Labor Trend,* 26-29, *https://www.jil.go.jp/kokunai/blt/backnumber/2008/11/026-029.pdf*, accessed November 29, 2025.
[10] Murata, M., Kurokawa, S., Ohnishi, O., Uneda, M., Doi, T. (2012). Real-time evaluation of tool flank wear by in-process contact resistance measurement in face milling, *Journal of Advanced Mechanical Design, Systems, and Manufacturing,* Vol. 6, No. 6, 958-970, doi: 10.1299/jamdsm.6.958.
[11] Gouarir, A., Kurokawa, S., Sajima, T., Murata, M. (2016). In-process tool wear detection of uncoated square end mill based on electrical contact resistance, *International Journal on Automation Technology,* Vol. 10, No. 5, 767-772, doi: 10.20965/ijat.2016.p0767.
[12] Gouarir, A., Kurokawa, S., Sajima, T., Murata, M. (2019). Influence of coating in square end mill using in-process tool wear detection based on electrical contact resistance, *International Journal on Automation Technology,* Vol. 13, No. 1, 125-132, doi: 10.20965/ijat.2019.p0125.
[13] Holm, R. (1967). *Electric contacts: Theory and application,* 4th Edition, Springer-Verlag, New York, USA, doi: 10.1007/978-3-662-06688-1.
[14] Holm, R. (1970). Constriction resistance of an assembly of elongated a-spots, In: *Proceedings of the International Conference on Electrical Contacts,* 16-18.
[15] Murata, M., Koga, Y., Gouarir, A., Kurokawa, S. (2023). In-process tool flank wear identification in face milling using Holm's contacts theory, *Journal of Advanced Mechanical Design, Systems, and Manufacturing,* Vol. 17, No. 5, JAMDSM0060, doi: 10.1299/jamdsm.2023jamdsm0060.
[16] Murata, M., Kurokawa, S., Yamaguchi, T. (2024). Speeding up of tool-work electrical contact resistance measurement, In: *Proceedings of the 3rd Australian Conference on Industrial Engineering and Operations Management,* Sydney, Australia, 19-31, doi: 10.46254/AU03.20240021.
[17] Hirano, F., Ohta, E. (1957). On the measurement of the electrical resistance of oil film in the rolling bearing, (in Japanese), *Transactions of the Japan Society of Mechanical Engineers,* Vol. 23, No. 134, 705-710, doi: 10.1299/kikai1938.23.705.
[18] Koga, Y., Murata, M. (2025). Application of tool-work contact electrical resistance measurement to flat end milling, In: *Proceedings of the 11th International Conference on Automation, Robotics, and Applications,* Zagreb, Croatia, 328-333, doi: 10.1109/ICARA64554.2025.10977639.
[19] Saitoh, Y., Iida, K., Sawada, S., Shimizu, K., Hattori, Y. (2007). Dependency of contact resistance on load, In: *Proceedings of the 53rd IEEE Holm Conference on Electrical Contacts*, Pittsburgh, USA, 70-75, doi: 10.1109/HOLM.2007.4318197.
[20] Tungaloy Corporation. General catalog: Turning-Grooving - All chapters (Metric), from *https://tungaloy.com/pdfviewer/gc_2023-2024_g_turning-grooving/*, accessed November 29, 2025.
[21] Öpöz, T., Chen, X. (2016). Chip formation mechanism using finite element simulation, *Strojniški Vestnik – Journal of Mechanical Engineering,* Vol. 62, No. 11, 636-646, doi: 10.5545/sv-jme.2016.3523.
[22] Li, A., Zang, J., Zhao, J. (2020). Effect of cutting parameters and tool rake angle on the chip formation and adiabatic shear characteristics in machining Ti-6Al-4V titanium alloy, *The International Journal of Advanced Manufacturing Technology,* Vol. 107, 3077-3091, doi: 10.1007/s00170-020-05145-9.